5

Application of Wavelength Dispersive X-Ray Spectroscopy in X-Ray Trace Element Analytical Techniques

Matjaž Kavčič
J. Stefan Institute
Slovenia

1. Introduction

The basic purpose of the x-ray trace element analytical techniques is to detect with high sensitivity elemental constituents of the target (including elements in trace amounts) and determine quantitatively the elemental composition of the investigated sample. These techniques are based on the detection of x-rays following the atomic inner shell ionization. An inner shell (core) electron can be removed from the atom in different ways, for the analytical purposes x-ray absorption and proton scattering are most commonly used. In the case of X-Ray Fluorescence (XRF) method the x-ray tube is usually applied to irradiate the sample while in the case of Proton Induced X-ray Emission (PIXE) the proton beam accelerated by the electrostatic accelerator to typical energy of MeV is used to ionize the target atoms. The atom with a hole in the inner shell (core hole) is extremely unstable with characteristic lifetime in the order of 10^{-15} s. Consequently, the inner shell ionization is followed via subsequent x-ray or Auger electron emission. Both, PIXE and XRF method exploit the radiative decay channel. The energy of the emitted x rays is given by the energy difference of the electron states involved in the transition which is characteristic of the target element atomic number. In order to identify the elemental composition of the target, energy analysis of the emitted radiation is required with energy resolution high enough to resolve characteristic spectral contributions from different elements in the sample. Such resolution is achieved by the energy dispersive solid state detectors in which electric signals are proportional to the incident x-ray energy and they are commonly used in x-ray trace element analytical techniques. Besides good enough energy resolution they also provide an excellent efficiency, which is crucial to collect weak signals from trace elements in the sample. It was in fact the development of the semiconductor detectors in the seventies that has triggered the development of x-ray analytical techniques. Today both PIXE and XRF techniques being a multi-element, sensitive, fast, non destructive and relatively inexpensive, have established as a routine analytical tool in a variety of fields such as material analysis, environmental and biomedical research, archeological and art studies,…

However, in some special cases the energy resolution of solid state energy dispersive detectors, nowadays reaching the order of 130 – 150 eV for the x-ray energies of few keV, is not enough and significantly higher energy resolution is required to enhance the analytical capabilities of the x-ray techniques. In order to increase further the energy resolution of x-

ray detection a wavelength dispersive x-ray (WDX) spectroscopy is usually applied. In this case x-rays are analyzed according to their wavelength using the Bragg diffraction on the crystal plane. While WDX spectroscopy has been traditionally used in combination with the electron excitation for major and minor element analysis it has usually not been considered in PIXE and XRF trace element analysis mainly due to low detection efficiency. Compared to the simplest wavelength dispersive spectrometers employing flat crystals the efficiency was enhanced significantly in modern spectrometers employing cylindrically or even spherically curved crystals in combination with position sensitive x-ray detectors. The energy resolution of such a spectrometer may exceed the resolution of the energy dispersive detector by two orders of magnitude while keeping the efficiency at a high enough level to perform trace element analysis.

In this chapter we will address two particular issues where we can apply successfully the WDX spectroscopy in order to enhance the capabilities of the x-ray trace element analytical techniques. The first part of the chapter deals with the chemical speciation of some light elements (P, S) via high resolution x-ray emission measurements. In the second part we will discuss the improvement of the detection limits in the case of analysis of trace elements with atomic number neighboring the predominant matrix element. In both cases the limiting factor is actually the restricted energy resolution of the energy dispersive solid state detectors. Application of WDX spectroscopy with energy resolution reaching towards the natural linewidths of the measured spectral lines overcomes this limitation and spreads the analytical capabilities of the x-ray techniques even further.

2. Chemical speciation of light elements via high resolution x-ray emission measurements

While PIXE and XRF technique yield with high accuracy elemental concentrations they are not sensitive to the chemical environment of the x-ray emitting atom and consequently they can not provide the chemical speciation of the elements in the sample. The most commonly used x-ray spectroscopic technique to perform chemical speciation is probably the x-ray absorption spectroscopy (XAS), which probes directly the unoccupied states just above the Fermi level. Experimental requirement for XAS spectroscopy is of course an intense monochromatic tunable x-ray source, which is available by a synchrotron. On the other hand x-ray emission spectroscopy (XES) probes the occupied states below the Fermi level. If we can achieve the energy resolution in the emission channel comparable to the resolution of the synchrotron beamline monochromator, information complementary to absorption spectra is expected from the high resolution XES spectra for the case of core-valence electron transitions. This principle is nicely illustrated in Figure 1 representing the direct comparison of the S K edge XAS spectrum and the Kβ emission spectrum recorded with the high energy resolution. Similarly as for the absorption spectrum the chemical environment of an element affects and modifies also the various characteristics of its x-ray emission spectrum. Usually, the influence of the chemical environment results in energy shifts of the characteristic lines, formation of satellite lines and changes in the emission linewidths and relative intensities (Gohshi et al. 1973, Perino et al. 2002, Tamaki 1995, Yasuda et al. 1978). A very important qualitative difference with the XAS spectroscopy requiring synchrotron source is that the x-ray emission spectrum can be recorded also in a smaller laboratory employing an x-ray tube (XRF) or proton accelerator (PIXE) in combination with wavelength dispersive x-ray spectrometer. Provided that the energy resolution of the x-ray emission spectrometer is high

enough a quantitative chemical state analysis is therefore feasible also in a small scale laboratories as it was demonstrated for the first time by Gohshi and co-workers by means of a double crystal spectrometer (Gohshi & Ohtsuka 1973). In order to perform chemical state analysis of trace elements in the sample a single crystal focusing type spectrometer is advantageous due to higher efficiency, which is crucial to collect weak signal from the sample.

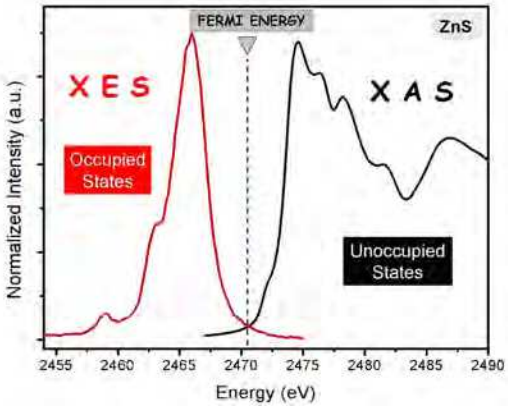

Fig. 1. S K-edge x-ray absorption near edge (XANES) spectrum and high resolution Kβ emission spectrum of ZnS (sphalerite) (Alonso Mori et al. 2010).

2.1 Experimental set-up

Here we present the wavelength dispersive x-ray spectrometer constructed and built at the J. Stefan Institute (Kavčič et al. 2004, Žitnik et al. 2009) that has been used extensively in the last couple of years to perform high resolution XES studies. The spectrometer is equipped with the cylindrically curved crystal in Johansson geometry, the Rowland circle radius is 50 cm.

Fig. 2. Inside view of the J. Stefan Institute's WDX spectrometer vacuum chamber with the target holder on a goniometer, crystal holder, and the CCD camera. A mechanical theta/2theta stage serves to adjust the Bragg angle.

The target holder, which is positioned well inside the Rowland circle, is mounted on the special custom made goniometer enabling two separate perpendicular translations (within beam direction and perpendicular to it) as well as rotation around vertical axis. The target goniometer serves for precise alignment of the target within the Rowland circle. The position of the target inside the Rowland circle closer to the crystal analyzer has two main advantages. First it enables efficient collection of x-rays emitted from large (extended) x-ray source without any loss of resolution. The second important point is that in combination with position sensitive x-ray detector it enables collection of diffracted x-rays over certain bandwidth given by the detector size. In our case the diffracted x-rays are detected by a Peltier cooled charged coupled device (CCD) detector, with dimensions 17.3 x 25.9 mm^2. The detector consists of 770 x 1152 pixels each having a size of 22.5 x 22.5 μm^2. The typical working temperature is -40 °C. Generally, the diffracted x-rays detected by the CCD detector form a two dimensional image on the detector plane. This image is projected on the horizontal axis corresponding to the energy axis of the spectrum. The spectrometer is equipped with three crystals, Quartz (1010) crystal with 2d lattice spacing of 8.510 Å, a Si(111) crystal with 6.271 Å, and a Si(220) crystal with 3.840 Å respectively. The whole spectrometer is enclosed in a 1.6 x 1.3 x 0.4 m^3 stainless-steel chamber evacuated by a turbomolecular pump down to 10^{-6} mbar. The proton incidence and x-ray emission angles are perpendicular to each other. With a given mechanics the Bragg angles of ~ 30^0 – 65^0 can be reached, this range being constrained by the size of the vacuum chamber. With the crystals mentioned above the energy range of 1.6 – 6.5 keV can be reached in first order of reflection.

The main characteristic of such wavelength dispersive setup is the energy resolution, which should, combined with good enough efficiency, enable the chemical speciation of elements in the sample. Figure 3 shows the Kα emission spectrum of yellow sulfur recorded after excitation with the 2.52 keV monochromatic photon beam. The $K\alpha_{1,2}$ doublet due to spin orbit splitting of the 2p shell, which is slightly above 1 eV is clearly resolved in the measured spectrum. The energy resolution is estimated to ~ 0.3 - 0.4 eV, which is well below the natural linewidth of the measured line at 0.61 eV (Campbell & Papp 2001). At such high experimental resolution the spectrum exhibit almost pure Lorentzian lineshape.

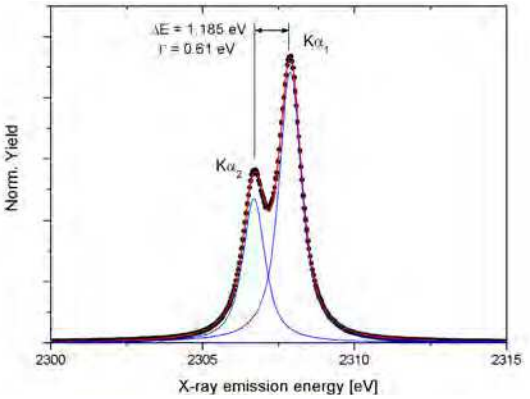

Fig. 3. High resolution Kα x-ray emission spectrum of yellow S excited by a monochromatic focused (200 x 50μm^2) photon beam with an 2.52 KeV energy. The spectrum was recorded at the ID26 beamline of the ESRF synchrotron using the wavelength dispersive spectrometer of the J. Stefan Institute.

The experimental setup enables detailed studies of fine structure within the XES spectra and accurate measurements of the energy shifts at the order of tenths of eV, which is relevant for the quantitative chemical speciation studies.

2.2 Chemical speciation of light elements via high resolution Kα XES measurements

As already explained in the introduction the core hole state induced by the proton scattering or photon absorption is unstable and decay via radiative or Auger transition. In case of 1s ionized atoms the fluorescence exhibit characteristic K x-ray lines. The most intense K spectral line named Kα corresponds to the 2p to 1s electron transition (core-core transition). Since only core electrons are involved in the transition it is generally expected that Kα spectral lines should be mostly free from chemical bond effects except from small energy shifts. These shifts are related to the valence electron population only indirectly through slight changes in the screening of the effective nuclear potential. We have performed extensive study of the energy shifts of the Kα lines for the various S compounds using excitation with monochromatic photon beam (Alonso Mori et al. 2009) and also MeV proton excitation (Kavčič et al. 2004, 2005). While the shape of the spectrum is not affected by the chemical environment, clear energy shifts of the measured Kα spectral lines are observed and they can be correlated directly with the oxidation state of sulfur in the sample (Figure 4). The energy position of the Kα line enables therefore a simple and reliable determination of the sulfur oxidation state.

In the next step the high resolution measurement of the Kα line energy is applied for the chemical state analysis of sulfur in a typical sample used in the analytical work. High resolution PIXE analysis of sulfur in an aerosol sample was chosen since PIXE is well established and commonly used method to determine the elemental concentrations in aerosol samples collected under specific time and particle size constraints. Among different elements in the atmosphere sulfur and its compounds present one of the most important pollutants in the atmosphere with the anthropogenic emission to account for the 75% of the total. The chemical reactivity and consequently its impact on the environment depend on the chemical state of sulfur so the information of oxidation state of sulfur in aerosol samples

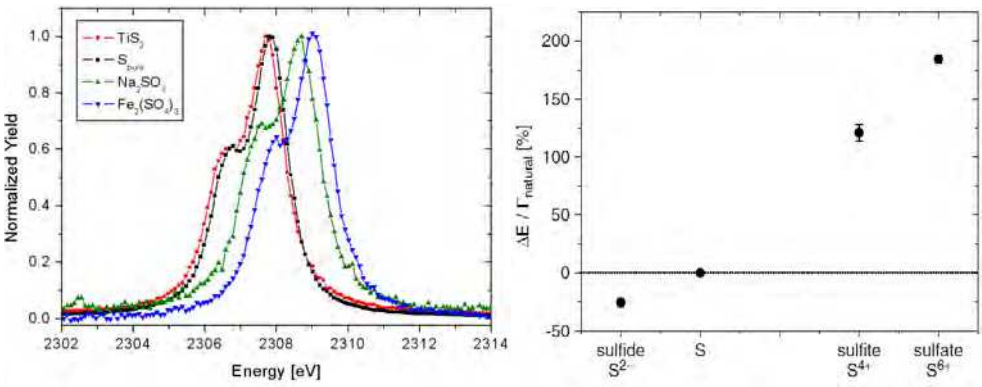

Fig. 4. (left) High resolution proton induced Kα x-ray emission spectra of several S compounds (Kavčič et al. 2004). (right) Measured energy shifts versus the oxidation state of S in the target. The energy shifts are given in units of the natural linewidth of the principal Kα line. A linear dependence of the Kα energy shift on the S oxidation state can be observed (Kavčič et al. 2005).

is highly relevant. Our measurements were performed on the aerosol sample collected on a Pallflex (2500Q AT-UP) tissue quartz filter using a 'Ghent type' sampling station. The total aerosol loading mass was ~ 0.4 mg/cm^2. The total S concentration of this specific sample was determined by the standard PIXE technique as 28.1 μg/cm^2. The measurements were performed at the Microanalytical Centre of the J. Stefan Institute in Ljubljana using the 2 MV tandem proton accelerator. The sample was exposed to 2 MeV proton beam with the 50 nA proton current. The measured Kα signal of sulfur in the sample is presented in Figure 5. The energy shift of the $K\alpha_{1,2}$ doublet was determined as 1.19 ± 0.06 eV. According to the Kα diagram energy shifts measured previously for various S compounds, the chemical state of sulfur in the aerosol sample was identified as a sulfate ($[SO4]^{2-}$).

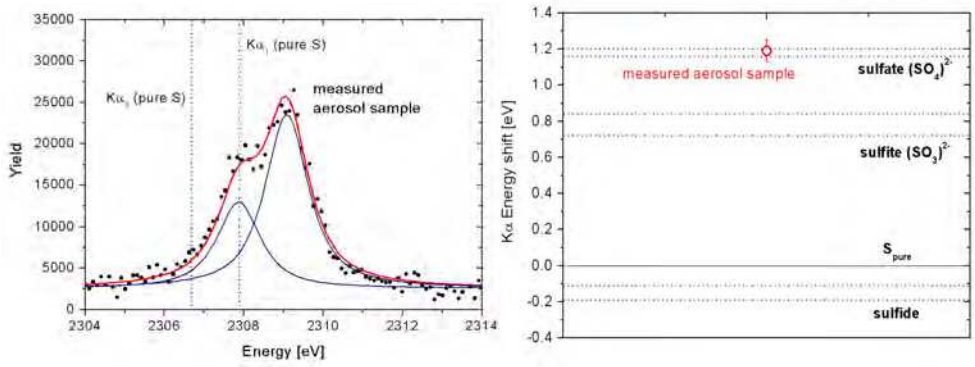

Fig. 5. (left) High-resolution proton-induced S Kα x-ray (HR-PIXE) spectrum from an aerosol sample (yield represents raw, digitized data from the detector's A/D converter; absorption of one S Kα photon corresponds to ~ 70 counts) and (right) graphical presentation of the chemical state speciation of S in aerosols employing HR-PIXE measurements of the S Kα diagram line. For each measured chemical state of sulfur, the horizontal lines define the discriminating ability of the HR-PIXE setup (Kavčič et al. 2005).

The same method can be applied also to other light elements. Recently we have performed a high resolution PIXE study on several P compounds in order to establish and apply the PIXE-based wavelength dispersive spectroscopy to determine the chemical state of various phosphorus compounds. The phosphorus is the key element in soil and bio-solid science. The speciation of P-mixtures is extensively studied in many aspects in order to understand the relationship between its chemical state and rate-reactivity, long-term solubility and accumulation, mobility and transfer to ground water. A similar procedure as in the case of sulfur was followed also for the case of P compounds. As the energy of the emitted fluorescence is slightly lower in this case the Quartz(1010) crystal was employed in the spectrometer to record the P Kα lines. Also in this case the target fluorescence was induced with the 2 MeV proton beam. The recorded Kα spectral lines for different P compounds with oxidation states ranging from -3 to +5 are presented in Figure 6. Also in this case clear energy shifts are observed, which are again correlated directly to the oxidation state of P in the sample. The extracted dependence is well reproduced by a linear fit as also shown in Figure 6.

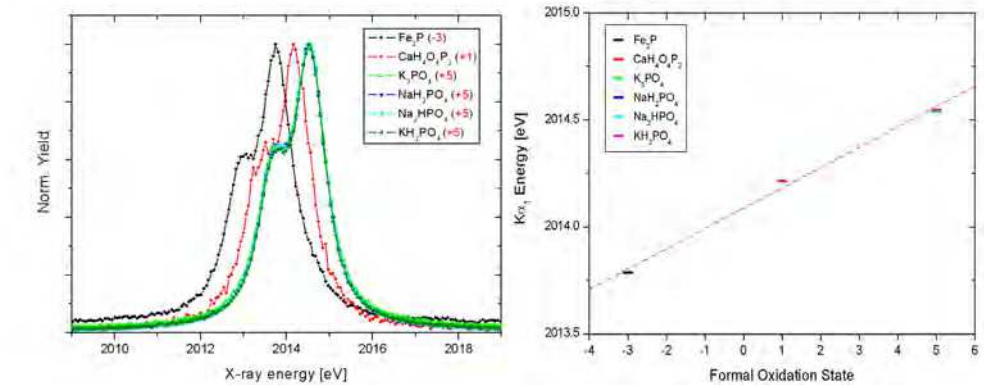

Fig. 6. (left) High-resolution proton-induced P Kα x-ray spectra from several P compounds. (right) Similar as for the S compounds a linear dependence of the Kα energy shift on the S oxidation state can be observed (Szlachetko & Kavčič 2011)

Based on this we can conclude that high resolution Kα x-ray emission measurements serve as a kind of chemical "ruler" for low Z elements oxidation. The spectral shape is practically independent on the oxidation state making the analysis simple and robust. A simple linear combination deconvolution procedure can be applied to mixed-valence system to perform also a quantitative study of the compound mixtures (Kavčič et al. 2004). The Kα line represent the strongest K x-ray spectral component which can be detected also for elements in low concentrations making it therefore feasible to perform chemical speciation of minor and trace elements in the sample.

2.3 Chemical and structural analysis of light elements via high resolution Kβ XES measurements

Compared to the Kα diagram line, which corresponds to the core–core (1s - 2p) transition the Kβ emission lines of light elements originate from valence-core transition. The high resolution Kβ emission measurements probes directly the p-density of occupied valence states and should therefore reflect with higher sensitivity the chemical environment of element in the sample. In fact most of the experimental as well as theoretical work on the chemical speciation of light elements, such as sulfur, has been focused on Kβ emission measurements (Kavčič et al. 2007, Maeda et al. 1998, Perino et al. 2002, Sugiura et al. 1974, Uda et al. 1999). All these works show pronounced effects in the emitted Kβ x-ray spectra, however, in contrast with the Kα spectra exhibiting independent characteristic lineshape the measured Kβ spectra are much more complex and consequently it is very difficult to give a simple parameter as it was the energy shift in the case of Kα spectra, which would correlate directly with the oxidation state and enable simple, reliable identification of the latter. Additional drawback is the fact that the Kβ line is much weaker than the Kα one making it more difficult to apply for chemical analysis of minor and trace elements. On the other hand the p-density of occupied valence states which is reflected in the emitted spectrum depend on the local coordination around central atom so using the theoretical modeling based on the quantum chemical calculations much more detailed analysis is possible yielding not only the oxidation state but also local coordination of ligand atoms.

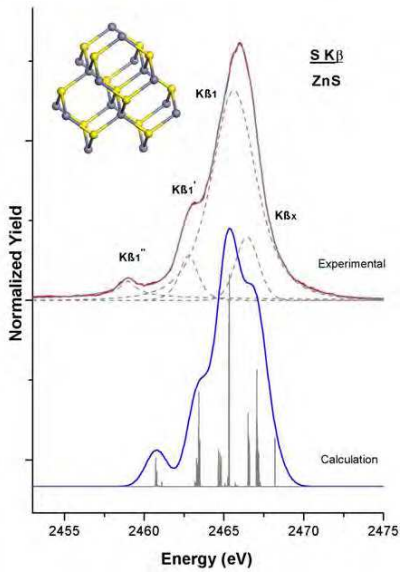

Fig. 7. S Kβ X-ray experimental spectrum of ZnS along with a 4.5Å cluster theoretical spectrum calculated within the density functional theory (DFT) (Alonso Mori et al. 2010)

We can therefore conclude that the high resolution Kβ x-ray emission spectra provide quantitative information about ligand environment. Comparison with the theoretically calculated spectra yields an opportunity to extract information about the electronic structure of element in the studied sample complementing this way the x-ray absorption near edge spectroscopy (XANES) used commonly at the synchrotron sources for this purpose.

3. Detection limits for trace elements with atomic number close to the target matrix element

One of the most important quantities for any x-ray trace element analytical technique is the minimum detection limit (MDL) yielding the minimum concentration of the trace element in the sample that we can detect. The principal factor governing the detection limits is the level of continuous background in the measured x-ray spectrum. Different physical processes contribute to this background. For charged particle excitation (electrons, protons, α particles) the bremsstrahlung from the projectile or secondary electrons and atomic bremsstrahlung (Ishii & Morita, 1984) are the most important sources of the continuous x-ray background. For heavier projectiles and higher energies the Compton tails of the γ-rays from nuclear reaction in the target specimen start to contribute significantly. When primary x-rays are used to excite the target (XRF method) the background in the measured spectra is produced mainly by elastic and Compton scattering of the primary photons. In this section we will discuss the analysis of trace elements with atomic numbers very close to the atomic number of the predominant matrix element. In this specific case the limitation comes from the strong x-ray fluorescence of the major matrix element which prevails the continuous x-ray background and represents a major limitation to detect a signal from neighboring trace

elements. In this case the MDLs are limited by the energy resolution rather than by the efficiency of the detection system. In order to drastically reduce the contribution of the tails of the dominant diagram lines from the target matrix element and consequently improve the detection limits the WDX spectroscopy can be successfully applied.
A typical example of such analytical problem comes from the field of archeology and cultural heritage. In the archeological studies of gold objects Pt and Pb, both with atomic numbers very close to Au, are among the most informative trace elements. Particularly Pt is extremely important since it provides information on the origin and provenance of ancient gold. Using standard proton induced x-ray emission (PIXE method), which is one of the most commonly applied techniques in this field, the detection limit of 2000 ppm was found for Pt. That was lowered to 1000 ppm by using selective Zn filter to absorb the Au L-lines but this value is still too high for most of the archeological needs. In order to further improve the detection limit, the energy selective photoexcitation (PIXE-XRF) was employed and the method was finally reported to achieve the 80 ppm detection limit (Guerra 2005). As expected, this value was constrained by the resonant Raman scattering on Au.
In our work the particular case of Pd and Cd in silver matrix was chosen to demonstrate the basic principle how the application of WDX spectroscopy helps to improve the detection limits for trace elements neighboring the target matrix element. Similar as gold also silver archeological objects are frequently studied by x-ray analytical methods (PIXE, XRF). Especially coins are objects of great historical value and x-ray based techniques can provide a proper determination of their manufacturing technology, age, authenticity and give useful information about the monetary history of a certain period (Rodrigues 2011). Pd and Cd are both archeologically relevant elements, Cd being particularly important for authenticity verification of silver antiques since it is being used as an additive in silver solders and alloys only recently and its presence clearly indicates a fairly modern origin of a silver alloy sample (Devos 1999).

3.1 Improved PIXE detection limits of Pd and Cd in silver matrix employing high resolution measurements of Lα spectral lines

Generally the absolute minimum detectable yield of the spectral contribution corresponding to particular target element is usually defined as

$$Y_{MDL} = 3\sqrt{bckgr} \tag{1}$$

where *bckgr* represents the background yield taken within the full width at half maximum (FWHM) of the measured line. In order to determine the minimum detectable yields for Pd and Cd we need to measure the widths of the corresponding Lα lines as well as the background level in the position of these lines. In order to determine quantitatively the MDLs that can be achieved for PIXE method employing WDX spectroscopy we have recorded the high resolution Lα x-ray emission spectra of pure Ag, Pd, and Cd target using our wavelength dispersive spectrometer (presented in section 2.1) yielding sub eV resolution. For this experiment the spectrometer was equipped with the Si(111) crystal and 3 MeV protons were used for target excitation. We have first recorded the Lα diagram line of a pure Ag target. Keeping the same target the spectrometer was tuned to the energy of the Pd and later also to the Cd Lα diagram line and the corresponding part of the

Ag x-ray spectrum was recorded (Fig. 8). The acquisition time for each measurement was set to 1000 seconds. After that the proton induced Lα diagram lines of Pd and Cd target were also recorded in order to determine the FWHM values (the acquisition time was reduced to 100 seconds) and compared directly with the corresponding x-ray spectral region collected on pure Ag target.

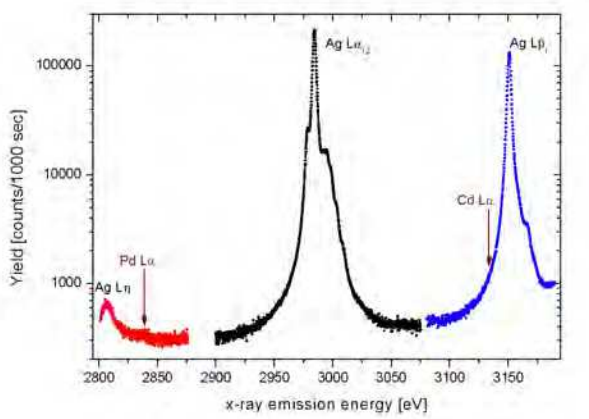

Fig. 8. High-resolution Ag Lα (L_3 – $M_{4,5}$) X-ray emission spectra induced with 3 MeV protons and the neighboring spectral regions centered around the energies of the Pd and Ag L lines. The Lβ$_1$ (L_2 – M_4) diagram line is situated in the high energy part of the measured spectrum and a weak Lη (L_2 – M_1) line is observed at the low energy edge. Arrows indicate the expected positions of the Pd and Cd Lα lines (Kavčič 2010).

The FWHM values of the Pd and Cd Lα line were determined by fitting the measured spectra with Voigt lines representing the Lorentzian natural lineshape convoluted with the Gaussian-like response of the spectrometer. Two Voigt profiles were used to model the Lα$_{1,2}$ lines. The proton induced spectra exhibit additional LM shell double ionization satellite structure on the high energy side of the diagram line which was fitted with several arbitrary Voigt profiles to account for the complex multiplet structure. The final result of the fitting procedure yielding the FWHM of the Lα$_1$ diagram line is presented in Figure 9. for Pd. In the next step the background level at the position of the expected Pd (or Cd) Lα signal was determined. The corresponding part of the measured proton induced Ag spectrum corresponding to the position of expected Pd signal was modeled by a single Voigt line representing the Ag Lη line (L_2-M_1 transition) and a constant background. The result of the fitting procedure which yielded the background level at position of the Pd line is also presented in Figure 9. A similar procedure that enables the determination of Y_{MDL} (Eq. 1) was followed also for Cd.

In order to reach final MDL values the absolute minimum detectable yields should be normalized relative to the absolute Lα yield from a pure target. In our analysis we have used the measured Ag Lα yield for normalization and than employ theory to scale appropriately this yield for each particular element (Pd or Cd). Theoretically the thick target Lα yield is given by

$$Y_{TT}^{proton} \propto \omega_{L_3} \frac{\Gamma_{La}}{\Gamma_{L_3}^{Rad}} \int_o^R \left[\sigma_{L_3}^I(E(x)) + f_{23}\sigma_{L_2}^I(E(x)) + (f_{12}f_{23} + f_{13} + f_{13}^{'})\sigma_{L_1}^I(E(x)) \right] e^{-\mu_{La}x} dx \quad (2)$$

where $E(x)$ is the proton energy as a function of the penetration depth, R the range of protons in the target, σ^I the L- subshell ionization cross sections, $\Gamma_{L\alpha}/\Gamma_L^{Rad}$ the relative emission rates for the $L\alpha$ radiative transition, f_{ij} Coster-Kronig (CK) yields and ω_3 the fluorescence yield for the L_3 subshell. The integration over x is usually converted into the energy integrals using the well known transformation $dx = dE / S(E)$, with S being the proton stopping power. We can calculate the Y_{TT} yield for any particular element using the corresponding ionization cross sections, emission rates and CK yields, while for the stopping power and attenuation we always consider the values for the Ag matrix. The scaling factor F^{th} is than given as a thick target yield Y_{TT} calculated for particular element (Pd, Cd) incorporated homogeneously in the Ag matrix relative to the value calculated for pure Ag target, which was used for normalization

$$F^{th} = \frac{Y_{TT}(Pd, Cd \text{ within } Ag \text{ matrix})}{Y_{TT}(\text{pure } Ag \text{ target})} \quad (3)$$

and the final MDL values are than obtained as

$$MDL = \frac{Y_{MDL}}{Y_{Ag} F^{th}} \quad (4)$$

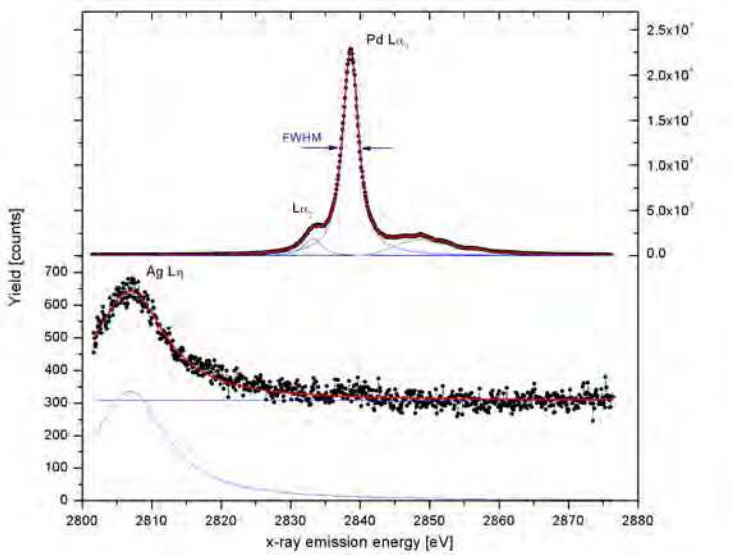

Fig. 9. (top) High-resolution Pd Lα X-ray emission spectrum induced with 3 MeV protons fitted with the model explained in the text in order to determine FWHM of the $L\alpha_1$ line. (bottom) Part of the high-resolution Ag Lα X-ray emission spectra corresponding to the energy region of the Pd Lα line. The Ag signal level defines the minimum detectable yield of Pd. (Kavčič 2010).

The final detection limits obtained from our high resolution proton induced Lα x-ray emission measurements are summarized in Table 1, together with the Y_{MDL} and FWHM values extracted from the measured Lα spectra, as well as calculated F^{th} scaling factors. For Pd very low MDL value reaching only 40 ppm was obtained, which is a direct consequence of excellent experimental energy resolution. In case of Cd slightly larger value of MDL was obtained (~60 ppm) mainly due to the proximity of Ag $L\beta_1$ line whose tail extends to the region of Cd Lα line.

These detection limits can be compared directly with the corresponding values obtained in the standard PIXE analysis based on energy dispersive detectors. The latter were obtained using the model Pd/Ag PIXE spectra collected with Si(Li) detector within our standard PIXE set-up by adding a short accumulation of Pd signal to the long accumulation of Ag. These model spectra were evaluated with the GUPIX program package (Maxwell et al. 1989) yielding also limits of detection for each particular element. Consistent detection limits were obtained four all four model PIXE spectra combining Ag (1000 sec) and Pd spectra with different exposition times (10, 20, 30, 50 sec) yielding final detection limit for Pd in Ag of 1140ppm ± 10ppm. Despite the fact that the K x-ray lines were used to obtain this result, as it is usually the case in standard PIXE analysis of mid-Z elements, this value is still almost 30 times larger than the corresponding detection limit obtained from Lα x-ray spectra collected with wavelength dispersive x-ray spectrometer.

Finally the same procedure was used to produce a model Pd/Ag spectrum this time recorded by a WDX spectrometer. One single CCD exposition (1 sec) collected from Pd target was added to the total Ag spectrum corresponding to total exposition time of 1000 seconds producing a model spectrum which can serve as a close approximation to the spectrum recorded on a standard sample with 1000 ppm of Pd within Ag matrix. While Pd signal is below the detection limit of standard PIXE analysis we have determined previously, the high resolution model spectrum presented in Figure 10 exhibit strong Pd signal demonstrating directly the capability to detect concentrations well below this level by applying WDX spectroscopy.

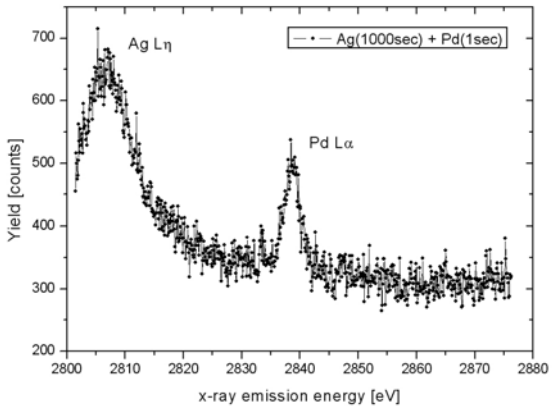

Fig. 10. A model high resolution PIXE spectrum measured with the WDX spectrometer. The spectrum was obtained by adding spectra from Ag and Pd target with exposition times of 1000 and 1 second, respectively (Kavčič 2010).

	Pd	Cd
Y_{MDL} [counts]	292 ± 2	477 ± 8
FWHM [eV]	2.78 ± 0.06	3.04 ± 0.10
F^{th}	0.974	1.040
MDL [ppm]	**39.8 ± 0.4**	**61.0 ± 1.1**

Table 1. The PIXE minimum detection limits (MDL) for Pd and Cd within the Ag matrix achieved by applying WDX spectroscopy. Given errors are calculated considering the background, Y_{Ag} and the Lα FWHM fitting errors. Tabulated are also minimum Pd and Cd detectable yields, FWHMs of the measured Lα spectra, and also calculated values of the scaling factor F^{th} used to obtain final detection limits.

3.2 Further improvement of detection limits achieved by combining a WDX spectroscopy with the tunable monochromatic synchrotron radiation

For trace elements with atomic number just below the matrix element, very good detection limits can be achieved using the tunable synchrotron radiation with excitation energy tuned below the absorption edge of the matrix element. In this case the majority of the unwanted fluorescence signal is eliminated, but there remains a part of it due to the resonant Raman scattering (RRS) on the target matrix element (Jaklevic et al. 1988). Also in this case the background due to the RRS signal can be removed effectively by applying the WDX spectroscopy. We have therefore performed additional high resolution measurements on Ag and Pd employing the tunable monochromatic synchrotron radiation. Two different photon beam energies were employed for excitation, namely 3400 eV, being well above the L_3 absorption edge of both Ag and Pd, and 3172.8 eV corresponding to the top of the strong photoexcited resonance at the L_3 absorption edge of Pd. To locate the resonance, L_3 absorption spectrum of Pd was previously recorded in the fluorescence mode. The Pd Lα spectra were then recorded at both selected energies, and finally also the part of the spectrum from the Ag target at excitation energy 3172.8 eV, corresponding to the maximum of the Pd L_3 cross section (Figure 11). The overall acquisition time for this measurement was 4000 s.

As a direct consequence of high energy resolution of the measured x-ray emission and the proper choice of photon probe energy the resonant Raman scattering (RRS) signal from Ag is effectively separated from the region of the expected Pd signal (Fig. 11). The remaining almost flat background originates mainly from the scattering of the strong primary photon beam. Unfortunately, the Ag target foil used in the photon probe measurements was slightly contaminated with Cl, which is manifested by the relatively strong Cl Kβ peak around 2816 eV. In order to determine the background level at the position of the expected Pd Lα signal, which is needed to extract the MDL, we have fitted the part of the spectrum above the Ag RRS signal with the combination of flat background, the Pd $L\alpha_{1,2}$ profile as obtained from the spectrum of Pd target and an additional peak to account for the Cl impurity Kβ line. The result of this fit yielding the background level needed to extract the minimum detectable yield (Equation 1) is presented in Figure 11. Besides the background level also the FWHM of the Pd $L\alpha_1$ line is needed and was determined by fitting the measured Pd Lα spectrum with Voigt lines similar as in the case of proton excitation. Compared to proton induced spectra a

significantly smaller FWHM was obtained. This is partly due to slightly better experimental resolution originating from the very small focused photon beam, but most of the broadening of the proton induced Lα lines is due to the strong LN shell multiple ionization induced by proton beam resulting in the line broadening. The final MDL was deduced using the same procedure as for the PIXE measurements (Equations 1, 3, 4). The only difference is the theoretical thick target yield which is in case of excitation with the monochromatic photon beam given by

$$Y_{TT}^{photo} \propto \omega_{L_3} \frac{\Gamma_{La}}{\Gamma_{L_3}^{Rad}} \left(\sigma_{L_3}^{ph}(E_{ph}) + f_{23}\sigma_{L_2}^{ph}(E_{ph}) + (f_{12}f_{23} + f_{13} + f_{13}^{'})\sigma_{L_1}^{ph}(E_{ph}) \right) \frac{1}{\mu_{matrix}^{E_{ph}} + \mu_{matrix}^{L\alpha}} \quad (5)$$

In this equation E_{ph} is the energy of the photon beam, σ^{ph} corresponds to L-subshell photoionization cross sections and μ_{matrix} denotes the attenuation coefficient of the target matrix for the incoming ($\mu^{Eph}{}_{matrix}$) and outgoing ($\mu^{L^{\alpha}}{}_{matrix}$) photon energies. The finally extracted MDL value is given in Table 2 together with the minimum detectable yield and the FWHM of the photoinduced Pd $L\alpha_1$ line. Tabulated is also the scaling factor calculated as a theoretical thick target yield for Pd in Ag matrix induced with 3172.8 eV photon beam relative to the yield of pure Pd excited with 3400 eV beam used for normalization.

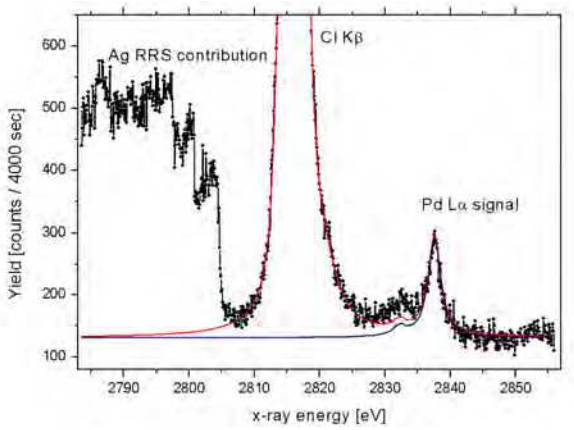

Fig. 11. The high resolution x-ray emission spectrum of Ag target measured after excitation with the 3172.8 eV photon beam tuned to the maximum of the Pd L_3 absorption edge. The Ag resonant Raman scattering contribution exhibiting characteristic high energy cutoff is completelly separated out of the region of the Pd Lα line. A strong signal at around 2816 eV corresponds to the Cl Kβ line and is due to the contamination of the Ag foil. An extremely high sensitivity of the set up is demonstrated by a clear signal corresponding to Pd, which is expected to be present in the Ag foil only in very low trace amount (Kavčič et al. 2011).

From the final MDL value given in Table 1 we can conclude that in the case of Z_{matrix} - 1 trace element (the case of Pd in Ag) the detection limits are improved even further compared to the previously determined PIXE detection limits. Finally the ppm level was reached by combining the WDX spectroscopy with the energy selective target photoexcitation. A small part of this improvement is achieved also on account of the extremely high photon flux but

most importantly, the WDX spectroscopy enables to separate completely the resonant Raman scattering signal from the Ag target at proper setting of the photon probe energy. The position of the characteristic high energy cutoff of the Ag RRS signal is clearly displayed in Figure 11 and its position depends linearly on the energy of the photon beam used for excitation. The energy displacement of this cutoff edge with respect to the position of Ag Lα fluorescence line corresponds to the actual energy detuning (the difference between the position of Ag L_3 absorption edge and the actual excitation energy). Since the lowest photon energy that can be used for such analysis is given by the Pd L_3 absorption edge, the energy difference between the Ag and Pd L_3 absorption edges (~ 178 eV (Deslattes et al. 2003)) sets the upper limit for this energy displacement. If we compare this value with the difference between Ag and Pd Lα fluorescence lines being ~ 146 eV (Deslattes et al. 2003) it is clear that a high energy resolution is mandatory to separate completely the two signals. It is very important to point out that this is a general problem in the analysis of $(Z\text{-}1)_{trace}$ / Z_{matrix} element combinations. It can be solved completely only by a combination of energy selective photoionization and WDX spectroscopy as demonstrated for the case of Pd/Ag combination reaching finally a minimum detection limits on the ppm level.

	Pd
Y_{MDL} [counts]	170 ± 1
FWHM [eV]	2.35 ± 0.01
F^{th}	2.55
MDL [ppm]	**1.37 ± 0.01**

Table 2. The minimum detection limit (MDL) for Pd within the Ag matrix obtained for excitation with monochromatic synchrotron radiation tuned just below the Ag L_3 edge. Tabulated are also minimum detectable yield, FWHM of the measured $L\alpha_1$ line, and also calculated value of the scaling factor F^{th} used to obtain final MDLs. The final error is calculated considering the background, Y_{Norm} and the Lα FWHM fitting errors.

4. Conclusion

The high resolution x-ray emission spectroscopy employing wavelength dispersive spectrometers with resolving power on the order of $E/\Delta E \sim 5000$ can be used efficiently in the x-ray trace element analytical techniques. At such resolution a chemical speciation can be performed in addition to the standard XRF and PIXE elemental analysis. The energy shifts of the Kα lines of several light elements depend linearly on the oxidation state and the measurement of the absolute energy can be exploited to determine the oxidation state of the element in the sample. The Kβ line reflects directly the p-density of occupied states and through comparison with the theoretically calculated spectra provides quantitative information about ligand environment. Therefore high resolution XES measurements with a modern wavelength dispersive spectrometer opens possibility to perform reliable chemical speciation studies also in the small laboratory employing x-ray tube or electrostatic proton accelerator for target excitation.

Another aspect where we can improve the performance of the x-ray analysis by applying the WDX spectroscopy is the detection sensitivity for the trace elements neighboring the

major target matrix element. A significant improvement of the detection limits for the case of Pd and Cd in silver matrix has been demonstrated. Because of extremely high experimental energy resolution reaching below the natural linewidths of the measured L x-ray lines, the detection limits of few tens of ppm were reached in case of proton excitation. For energy selective photoexcitation employing synchrotron radiation the detection limit for Pd was lowered even further. Due to high experimental energy resolution in both, the photon-in and photon-out channels, the Ag RRS contribution could be completely separated from the Pd signal yielding the final MDL value on the ppm level. This result demonstrates the general potential of WDX spectroscopy to obtain substantially lower detection limits for x-ray analysis of trace elements neighboring the target matrix element.

5. Acknowledgment

The author acknowledges the support of the Slovenian Ministry of Education, Science and Sport through the research program P1-0112. A part of the work on chemical speciation has been supported also by the European Community as an Integrating Activity 'Support of Public and Industrial Research Using Ion Beam Technology (SPIRIT)' under EC contract no. 227012.

6. References

Alonso Mori, R.; Paris, E.; Giuli, G.; Eeckhout, S. G.; Kavčič, M.; Žitnik, M.; Bučar, K.; Pettersson, L. G. M.; Glatzel, P. (2009) , Electronic Structure of Sulfur Studied by X-ray Absorption and Emission Spectroscopy, Analytical Chemistry Vol. 81, Issue 15, pp. 6516-6525

Alonso Mori, R.; Paris, E.; Giuli, G.; Eeckhout, S. G.; Kavčič, M.; Žitnik, M.; Bučar, K.; Pettersson, L. G. M.; Glatzel, P. (2010) , Sulfur-Metal Orbital Hybridization in Sulfur-Bearing Compounds Studied by X-ray Emission Spectroscopy, Inorganic Chemistry Vol. 49, No. 14, pp. 6468-6473

Campbell, J.L.; Papp, T. (2001), Widths of the atomic K-N7 levels, Atomic Data and Nuclear Data Tables, Vol. 77, Issue 1, pp 1-56

Deslattes, R.D.; Kessler E.G.; Indelicato, P.; De Billy, L.; Lindroth, E.; Anton, J. (2003), X-ray transition energies: new approach to a comprehensive evaluation, Reviews of Modern Physics, Vol. 75, Issue 1, pp. 35-99

Devos, W.; Moor, Ch.; Lienemann, P. (1999), Determination of impurities in antique silver objects for authentication by laser ablation inductively coupled plasma mass spectrometry (LA-ICP-MS), Journal of Analytical Atomic Spectroscopy, Vol. 14, Issue 4, pp. 621-626

Gohshi, Y.; Ohtsuka , A. (1973), The application of chemical effects in high resolution X-ray spectrometry, Spectrochimica Acta B, Vol. 28, Issue 5, pp. 179-188

Guerra, M.F.; Calligaro, T.; Radtke, M.; Reiche, I.; Riesemeier, H. (2005), Fingerprinting ancient gold by measuring Pt with spatially resolved high energy Sy-XRF, Nuclear Instruments and Methods in Physics Research B, Vol. 240, Issues 1-2, pp. 505-511

Ishii, K.; Morita, S. (1984), Continuum x rays produced by light-ion—atom collisions, Physical Review A, Vol. 30, Issue 5, pp. 2278-2286

Jaklevic, J.M.; Giaugue, R.D.; Thompson, A.C. (1988), Resonant Raman scattering as a source of increased background in synchrotron excited x-ray fluorescence, Analytical Chemistry Vol. 60, Issue 5, pp. 482-484

Kavčič, M.; Karydas, A.; Zarkadas, Ch. (2004), Chemical state analysis of sulfur in samples of environmental interest using high resolution measurement of Kα diagram line, Nuclear Instruments and Methods in Physics Research. B, Vol. 222, Issues 3-4, pp. 601-608

Kavčič, M.; Karydas, A.; Zarkadas, Ch. (2005), Chemical state analysis employing sub-natural linewidth resolution PIXE measurements of Kα diagram lines, X-Ray Spectrometry, Vol. 34, Issue 4, pp. 310-314

Kavčič, M.; Dousse, J.-Cl.; Szlachetko, J., Cao, W (2007), Chemical effects in the Kβ X-ray emission spectra of sulfur, Nuclear Instruments and Methods in Physics Research B, Vol. 260, Issue 2, pp. 642-646

Kavčič, M. (2010), Improved detection limits in PIXE analysis employing wavelength dispersive X-ray spectroscopy, Nuclear Instruments and Methods in Physics Research B, Vol. 268, Issue 22, pp. 3438-3442

Kavčič, M.; Žitnik, M.; Bučar, K.; Mihelič, A.; Szlachetko, J. (2011), Application of wavelength dispersive X- ray spectroscopy to improve detection limits in X-ray analysis, X-Ray Spectrometry, Vol. 40, Issue 1, pp. 2-6

Maeda, K.; Hasegawa, K.; Hamanaka H., Maeda, M. (1998), Chemical state analysis in air by high-resolution PIXE, Nuclear Instruments and Methods in Physics Research B, Vol. 136-138, pp. 994-999

Maxwell, J.A.; Campbell, J.L.; Teasdale, W.J. (1989), The Guelph PIXE software package, Nuclear Instruments and Methods in Physics Research. B, Vol. 43, Issue 2, pp. 218-230

Perino, E.; Deluigi, MT.; Olsina, R.; Riveros, JA. (2002), Determination of oxidation states of aluminium, silicon and sulfur, X-Ray Spectrometry, Vol. 31, Issue 2, pp. 113-187

Rodrigues, M.; Schreiner, M.; Melcher, M.; Guerra, M.; Salomon , J.; Radtke, M.;Alram, M.; Schindel, N. (2011), Characterization of the silver coins of the Hoard of Beçin by X-ray based methods, Nuclear Instruments and Methods in Physics Research B, doi:10.1016/j.nimb.2011.04.068

Sugiura, C; Gohshi, Y.; Suzuki, I. (1974) Sulfur Kβ x-ray emission spectra and electronic structures of some metal sulfides, Physical Review B, Vol. 10, Issue 2, pp. 338-343

Szlachetko, J.; Kavčič, M. (2011), to be published

Tamaki, Y. (1995), Chemical effect on intensity ratios of K-series x-rays in vanadium, chromium and manganese compounds, X-Ray Spectrometry, Vol. 24, Issue 5, pp. 235-240

Uda, M.; Yamamoto, T.; Tatebayashi T. (1999), Theoretical prediction of S Kβ fine structures in PIXE-induced XRF spectra, Nuclear Instruments and Methods in Physics Research B, Vol. 150, Issues 1-4, pp. 55-59

Yasuda, S.; Kakiyama, H. (1978), X-ray K emission spectra of vanadium in various oxidation states, X-Ray Spectrometry, Vol. 7, Issue 1, pp. 23-25

Žitnik, M.; Kavčič, M.; Bučar, K.; Mihelič, A. (2008), X-ray resonant Raman scattering from noble gas atoms and beyond, Nuclear Instruments and Methods in Physics Research B, Vol. 267, Issue 2, pp. 221-225

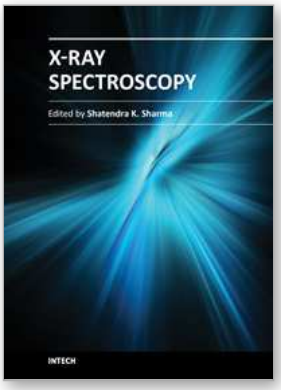

X-Ray Spectroscopy

Edited by Dr. Shatendra K Sharma

ISBN 978-953-307-967-7
Hard cover, 280 pages
Publisher InTech
Published online 01, February, 2012
Published in print edition February, 2012

The x-ray is the only invention that became a regular diagnostic tool in hospitals within a week of its first observation by Roentgen in 1895. Even today, x-rays are a great characterization tool at the hands of scientists working in almost every field, such as medicine, physics, material science, space science, chemistry, archeology, and metallurgy. With vast existing applications of x-rays, it is even more surprising that every day people are finding new applications of x-rays or refining the existing techniques. This book consists of selected chapters on the recent applications of x-ray spectroscopy that are of great interest to the scientists and engineers working in the fields of material science, physics, chemistry, astrophysics, astrochemistry, instrumentation, and techniques of x-ray based characterization. The chapters have been grouped into two major sections based upon the techniques and applications. The book covers some basic principles of satellite x-rays as characterization tools for chemical properties and the physics of detectors and x-ray spectrometer. The techniques like EDXRF, WDXRF, EPMA, satellites, micro-beam analysis, particle induced XRF, and matrix effects are discussed. The characterization of thin films and ceramic materials using x-rays is also covered.

How to reference

In order to correctly reference this scholarly work, feel free to copy and paste the following:

Matjaž Kavčič (2012). Application of Wavelength Dispersive X-Ray Spectroscopy in X-Ray Trace Element Analytical Techniques, X-Ray Spectroscopy, Dr. Shatendra K Sharma (Ed.), ISBN: 978-953-307-967-7, InTech, Available from: http://www.intechopen.com/books/x-ray-spectroscopy/application-of-wavelength-dispersive-x-ray-spectroscopy-in-x-ray-trace-element-analytical-techniques

INTECH
open science | open minds

InTech Europe
University Campus STeP Ri
Slavka Krautzeka 83/A
51000 Rijeka, Croatia
Phone: +385 (51) 770 447
Fax: +385 (51) 686 166
www.intechopen.com

InTech China
Unit 405, Office Block, Hotel Equatorial Shanghai
No.65, Yan An Road (West), Shanghai, 200040, China
中国上海市延安西路65号上海国际贵都大饭店办公楼405单元
Phone: +86-21-62489820
Fax: +86-21-62489821